Noise Characteristics of Operational Real-Time High-Rate GNSS Positions in a Large Aperture Network

Diego Melgar[1], Brendan W Crowell[2], Timothy Ian Melbourne[3], Walter Michael Szeliga[3], V. Marcelo Santillan[3], and Craig Scrivner[3]

[1]University of Oregon
[2]University of Washington
[3]Central Washington University

November 24, 2022

Abstract

Large earthquakes are difficult to model in real-time with traditional inertial seismic measurements. Several algorithms that leverage high-rate RT-GNSS positions have been proposed and it has been shown that they can supplement the earthquake monitoring effort. However, analyses of the long-term noise behavior of high-rate RT-GNSS positions, which are important to understand how the data can be used operationally by monitoring agencies, have been limited to just a few sites and to short time spans. Here we show results from an analysis of the noise characteristics of one year of positions at 213 RT-GNSS sites spanning a large geographic region from Southern California to Alaska. We characterize the behavior of noise and propose several references noise models which can be used as baselines to compare against as technological improvements allow for higher precision solutions. We also show how to use the reference noise models to generate realistic synthetic noise that can be used in simulations of HR-GNSS waveforms. We discuss spatiotemporal variations in the noise and their potential sources and significance. We also detail how noise analysis can be used in a dynamic quality control to determine which sites should or should not contribute positions to an earthquake modeling algorithm at a particular moment in time. We posit that while there remain important improvements yet to be made, such as reducing the number of outliers in the time series, the present quality of real-time HR-GNSS waveforms is more than sufficient for monitoring large earthquakes.

Noise Characteristics of Operational Real-Time High-Rate GNSS Positions in a Large Aperture Network

Diego Melgar[1], Brendan W. Crowell[2], Timothy I. Melbourne[3],Walter Szeliga[3], Marcelo Santillan[3], & Craig Scrivner[3]

[1]Department of Earth Sciences, University of Oregon, Eugene, OR
[2]Department of Earth and Space Sciences, University of Washington, Seattle, WA
[3]Geology Department, Central Washington University, Ellensburg, WA

Corresponding author: Diego Melgar (dmelgarm@uoregon.edu)

Key Points

- We study the noise behavior of 213 HR-GNSS sites from California to Alaska
- We characterize the spatiotemporal noise behavior and propose reference noise models
- The present real-time noise is low enough that GNSS can be used for monitoring earthquakes

Abstract

Large earthquakes are difficult to model in real-time with traditional inertial seismic measurements. Several algorithms that leverage high-rate RT-GNSS positions have been proposed and it has been shown that they can supplement the earthquake monitoring effort. However, analyses of the long-term noise behavior of high-rate RT-GNSS positions, which are important to understand how the data can be used operationally by monitoring agencies, have been limited to just a few sites and to short time spans. Here we show results from an analysis of the noise characteristics of one year of positions at 213 RT-GNSS sites spanning a large geographic region from Southern California to Alaska. We characterize the behavior of noise and propose several references noise models which can be used as baselines to compare against as technological improvements allow for higher precision solutions. We also show how to use the reference noise models to generate realistic synthetic noise that can be used in simulations of HR-GNSS waveforms. We discuss spatiotemporal variations in the noise and their potential sources and significance. We also detail how noise analysis can be used in a dynamic quality control to determine which sites should or should not contribute positions to an earthquake modeling algorithm at a particular moment in time. We posit that while there remain important improvements yet to be made, such as reducing the number of outliers in the time series, the present quality of real-time HR-GNSS waveforms is more than sufficient for monitoring large earthquakes.

1. Motivation

There is broad interest in the international earthquake monitoring community in high rate (HR, epoch length <= 1sps) real-time position estimation from Global Navigation Satellite Systems (GNSS) such as the Global Positioning System (GPS) and others. It has been shown that HR-GNSS displacement waveforms can supplement measurements from traditional seismic networks based on inertial sensors and can be leveraged to characterize moderate to large earthquakes in seconds to minutes. This interest arises because algorithms that rely on inertial sensors “saturate” for large events, particularly at local and regional distances (e.g. Hoshiba and Ozaki, 2014). Saturation means that large and very large events look similar in inertial recordings and cannot be distinguished from one another in the first minutes following a significant event. The exact causes for this are still a matter of some debate but are most likely that the long period band of ground motion (period >10s) is not faithfully recorded by strong motion sensors in the near-field. In contrast, this low frequency energy which distinguishes large events is recorded with fidelity by HR-GNSS from the Nyquist frequency out to and including static, or permanent, offsets. As a result, many researchers have studied and proposed algorithms based on HR-GNSS that compute magnitude [Melgar et al., 2015], focal mechanisms (faulting style) [Crowell et al. 2016, Riquelme et al. 2016], and slip distribution [Grapenthin et al. 2014, Minson et al., 2014; Kawamoto et al. 2016] in real- or near real-time. Several of these algorithms have been systematically evaluated with both real and simulated events and are being used to complement traditional seismic approaches in earthquake and tsunami early warning systems. Thorough reviews of these issues can be found in Bock & Melgar [2016] and Larson [2019].

Measurements of ground motion from HR-GNSS differ from those obtained by inertial seismic sensors in fundamental ways. In the electro-mechanical systems used in seismometry the digitized acceleration or velocity of a proof mass inside the instrument correlates directly, through a known transfer function, to the actual ground motion. HR-GNSS positions are a wholly different kind of derived product. As a space-based geodetic approach, calculation of HR-GNSS positions relies on measurement of the time of flight of a microwave transmission between a satellite and a ground based antenna and receiver as well as the phase with which the signal arrives. These measurements coupled with knowledge of ancillary variables such as transmission delays through the troposphere and ionosphere, knowledge of the satellite clocks and orbits, and others, are used by a positioning algorithm to solve a least squares problem and produce epoch by epoch *solutions* of the station coordinates in a particular reference frame. The most common reference frame is the International Terrestrial Reference Frame (ITRF) which satellite orbits are generally computed in [Altamimi et al.,2016]. If the GNSS antenna is firmly coupled to the ground through a geodetic monument and it experiences a sudden motion, such as the one produced by an earthquake, the position solutions can be used to obtain displacement waveforms in local topocentric north, east, and vertical components of that particular point of the surface of the Earth. While the concept behind GNSS positioning is in essence simple, the estimation of the position of the antenna phase center using satellite signals, the practice is complex, especially for high sample rates and in real-time. Satellite orbits and clocks which determine the spatial and temporal origin of the microwave signal used to solve for the position are not as well known in real-time as is necessary for precise positioning. As a result, a number of external corrections must be calculated using a reference regional network (e.g. Geng et al., 2013) and applied in real-time for the positions to achieve the cm-level precision needed for earthquake monitoring.

In spite of this seemingly added complexity when compared to inertial sensors, real-time HR-GNSS networks have proliferated to almost every tectonically active region (e.g. Barrientos & Perez-Campos, 2018) and a variety of methods are employed to calculate the GNSS positions. There exist proprietary software for positioning from a number of vendors as well as open source academic codes (e.g. Geng et al., 2019). However, in spite of the significant progress in positioning and in understanding how HR-GNSS can contribute to real-time earthquake monitoring as well the rapid expansion of real-time networks one important outstanding issue remains. What are the noise characteristics and long-term behavior and performance of the position solutions in a real-world setting across a network with large geographic aperture? Characterization of the actual real-time performance of HR-GNSS has only been performed in small scale controlled settings such as shaketables and on individual station to station baselines (e.g. Bock et al., 2000; Langbein & Bock, 2004; Genrich & Bock, 2006; Bock et al., 2011). Tests of real-time performance have also been carried out in a simulated mode post-hoc for large events [e.g. Fang et al., 2013]. Recently Melgar et al., [2019] studied the performance of 9 HR-GNSS stations that were recorded and positioned in real-time and broadcast to end users for the 2019 M6.4 and M7.1 Ridgecrest, California earthquakes. When compared to post-processed solutions it was found that the main features of the waveforms used for rapid source characterization, the peak ground displacement (PGD) and the coseismic offsets compared favorably between real-time and post-processed data. However, differences between real-time and post-processed positions were also apparent. Post-processed solutions are able to leverage final orbit and clock products as well as use iterative approaches and full time-series filtering to compute positions whereas RT-GNSS positions can only utilize recursive filters and rely heavily on phase ambiguity stability.

In this work we explore this issue further. We will study the long term noise characteristics of real-time 1Hz point position time series computed in the ITRF global reference frame by the Geodesy Lab at Central Washington University (CWU) for a network of 213 stations (Figure 1) spanning from southern California to Alaska. These data are streamed from the field site to CWU where positions are computed on the fly. The solutions are re-broadcast to a number of users including the U.S. Geological Survey and the National Oceanographic and Atmospheric Administration (NOAA). The data are streamed as well to the Universities of Oregon and Washington where they are analyzed and archived. Here we will discuss the temporal and spatial behavior of noise in these HR-GNSS solutions. We emphasize that the performance we aim to characterized here is by definition a snapshot in time. GNSS positioning technology is improving constantly and it is our hope that the noise models we will demonstrate can be used by others to benchmark improvements and progress. These proposed reference noise models can potentially be used to determine the quality of the positioning solutions from a particular positioning algorithm or at a particular station of interest. Finally, we will demonstrate how to use the reference models to generate synthetic time series of noise which can be added to simulations of earthquake ground motions to more accurately represent a real-world scenario and to test rapid source estimation methods.

2. Data and Analysis Method

2.1 Network and Positioning

Many continuous GNSS networks operate in the region spanned by this study (Figure 1, the U.S West Coast, Canada, and Alaska) and, while an exact figure on the number of available sites is hard to come by and changes frequently, it is likely on the order of ~1000 stations (e.g. Blewitt et al., 2018). Of these, a subset of 213 was chosen for a demonstration project for NOAA. This agency is interested in using GNSS to supplement its local tsunami warning effort and so, starting in 2017, positions for this subset of sites began to be streamed in real-time to the Tsunami Warning Centers in Hawaii and Alaska [Melbourne et al., 2018]. In order to analyze the performance of the data, starting in October 2018 the positions are also being streamed to the University of Oregon where they archived as individual daily station files in miniSEED format for later analysis.

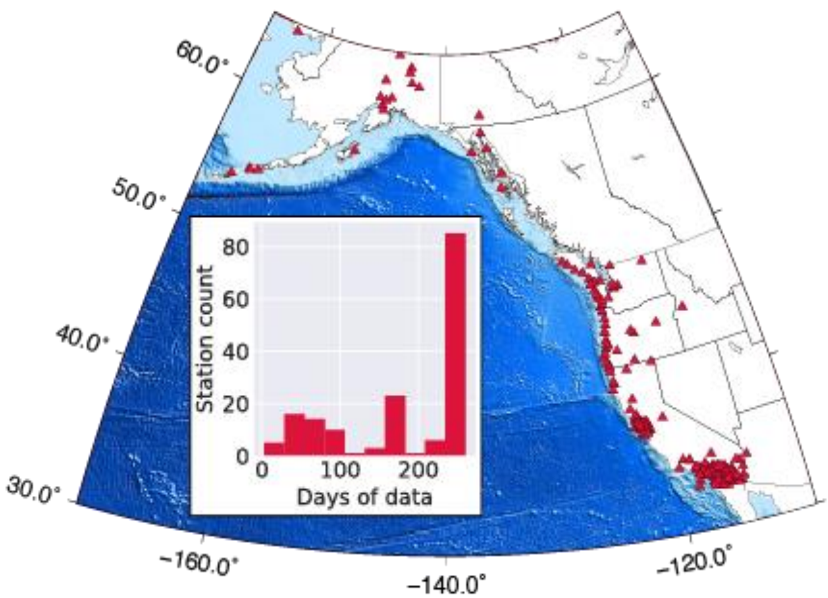

***Figure 1**. Distribution of real-time stations analyzed in this study. The inset histogram shows how many days of real-time data are available for each station.*

The positions themselves are produced by Central Washington University's *FastLane* algorithm. The raw GNSS data are telemetered from the field to the central location for a particular network operator such as Boulder CO for UNAVCO Inc. sites or Berkeley CA, for UC Berkeley stations. From there the individual network operators streams the data to

CWU in Ellensburg, WA where Fastlane computes the epoch by epoch position solutions and in turn serves them to other users such as NOAA and the UO.

The *Fastlane* positioning system [Santillan et al., 2013] produces precise point position (PPP, Zumberge et al., 1997) estimates based primarily on GNSS carrier phase observables (currently only from the GPS constellation) and satellite clock corrections provided by the Real-Time Service (RTS) of the International GNSS Service (IGS). The GPS carrier phase data is internally continuously calibrated using geometry free combinations of the L1 and L2 pseudorange and phase observables. This calibration step is a Kalman filter based algorithm that simultaneously estimates the best floating point ambiguities while monitoring and correcting for possible cycle slips. Fastlane uses GPS carrier phase based only, unlike other PPP algorithms (e.g. Kouba & Heroux 2001) that rely on both phase and pseudorange. This approach to PPP relies on the fact that the calibration procedure greatly mitigates the influence of code multipath that may affect the estimation of the floating point ambiguities. By using well calibrated data Fastlane uses only half the number of input observations therefore reducing the overall computation of the position estimates which also translates into smaller latencies. This approach is far less contaminated by multipath error, one of the largest sources of noise in high-rate positioning. Fastlane uses a highly efficient algorithm for the resolution of carrier phase initial ambiguities, which for most stations can be initially resolved in 20-30 seconds. After this the positions can be efficiently determined. Positions are computed in SI units (meters) in Earth Centered Earth Fixed reference frame (XYZ coordinates). Prior to streaming out the solutions to users these are rotated to a more familiar topocentric local north, east, and vertical reference frame. An example year-long waveform is shown in Figure 2.

2.2 Noise Analysis

First we study simple time domain features of the real-time waveforms such as the number and amplitude of outliers. For every station we count how frequently displacement levels of certain thresholds are exceeded in order to quantify the frequency of occurrence of the large displacement excursions seen in Figure 2. However, the bulk of our analysis focuses on the frequency domain. We employ the probabilistic power spectra (PPSD) technique of McNamara & Buland (2004) for all sites. The PPSD method is common in seismology to characterize the long term noise behavior of broadband sites. We take 20 min windows at each site and for each of the three components of motions and calculate the power spectra. This is repeated for every time window available for each site and an empirical probability density function (PDF) of the distribution of power at each frequency is obtained for every station. An example of the PPSD calculation for the same station in Figure 2 is shown in Figure 3. The PPSD approach is desirable because it minimizes the need to “fix” issues with the time series prior to calculating the spectra. As shown in Figure 2 there are outliers, steps, and spikes, as well as gaps in the data. The PPSD will naturally deal with these. A window with one of these behaviors will simply plot at a higher power. Meanwhile windows without these issues, which are more frequent, will eventually illuminate the median behavior as well as the lowest possible expected noise.

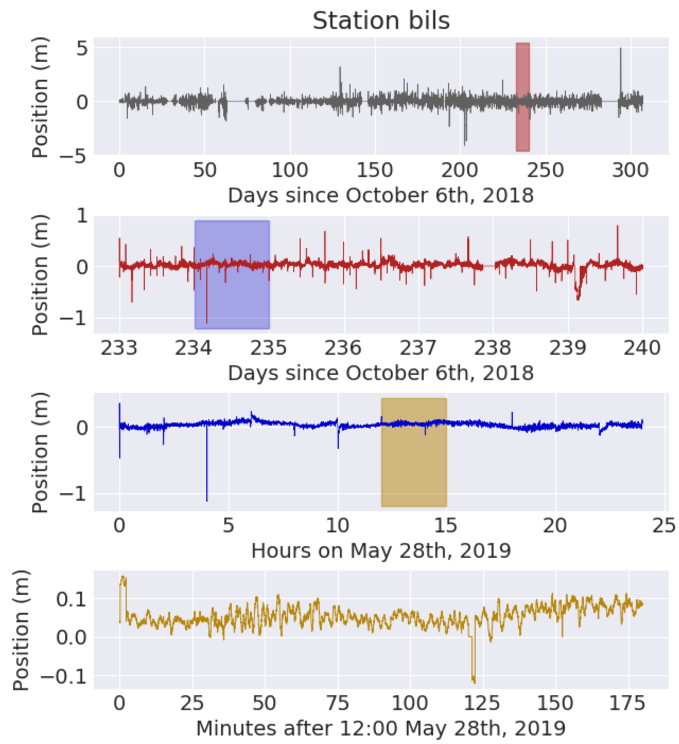

Figure 2. *Example time series for the east-west component of station BILS. Plotted are successive closeups of the data starting from the entire span and finishing with a three hour period.*

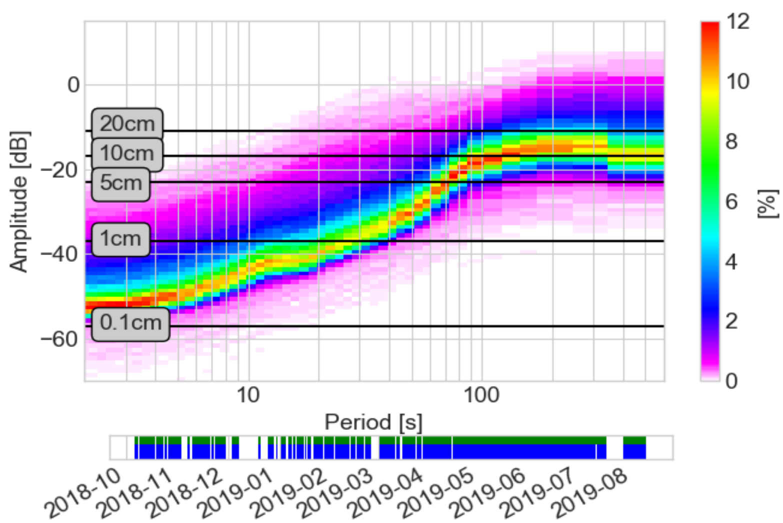

Figure 3. *Example PPSD for the east-west component of displacement of station BILS (Figure 2). The black lines are used as a reference and denote the power of a Gaussian white noise time series with the specified standard deviation. The bar at the bottom denotes the time-spans covered by the data.*

After we obtain PPSDs for each of the 213 sites in this study and for each component of motion we aggregate all of them to obtain the overall behavior of the HR-GNSS noise. From this regional PPSD we can extract reference noise models, for example, we select the 1th percentile from the regional PPSD and term this the “low-noise” model. Similarly the 50th and 90th percentiles of the PPSD are use to define the “median” and “high-noise” models.

2.3 Generation of synthetic noise time series

Using the regional reference noise models we demonstrate a simple method for generating synthetic time series of noise that recreate the behavior observed in the real data. We follow the approach first proposed by Boore [1983] and further detailed in Graves & Pitarka [2010] for generating stochastic time series in seismology. The approach has three simple steps, first, we create a Gaussian white noise time series with a specified sample rate (e.g. 1Hz) and duration. Second, we apply the Fourier transform to the white noise time series and keep the random phase spectrum but replace the white noise PSD with the reference noise model PSD. Finally we inverse Fourier transform to the time domain and recover a time series. While we have proposed three reference models at the 1th, 50th, and 90th percentiles, we have also extracted noise models for every 10th percentile. In the acknowledgments we provide links to code and a tutorial that demonstrates how to generate the synthetic time series.

3. Results

3.1 Overall noise characteristics

The time series in Figure 2 show seemingly meter-level accuracies in the positions, this is far too high to satisfy the cm- to decimeter requirement needed to monitor large events (e.g. Melgar et al., 2015; Ruhl et al, 2018), however if the data are plotted over shorter time scales we can see that this is the result of outliers and that in reality over time scales of minutes the data show cm-level precision. To further demonstrate this we take every 20min segment, remove its mean and count how frequently it exceeds displacement thresholds of certain levels. We do this for all sites and all epochs. The distribution of positions in the east direction and the cumulative density function are in Figure 4 and show that in spite of the outliers 90% of the data have noise smaller than 20cm.

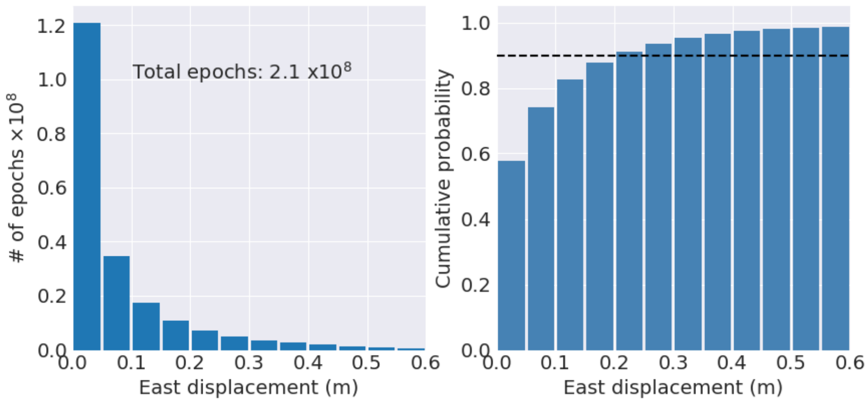

***Figure 4**. Number of outliers in the position waveforms in the east direction for different thresholds and for all sites and all epochs. The black dashed line in the cumulative density function is the 90% level.*

Figure 5 shows the aggregate PPSD plot for all three components of motion for all stations. We note that as first described by Genrich & Bock [2006] the real time positions have roughly red noise with a plateau at periods longer than ~100s and decreasing noise levels at shorter periods. The noise is generally lowest for the east component, followed by the north component, with the highest noise levels in the vertical direction. This is consistent with what is seen in post-processed data (e.g. Bock et al., 2011, Melgar et al., 2019) and is usually attributed to the geometry of the constellation of satellites. This is more clearly seen in Figure 6 where the 1th, 50th, and 90th percentiles of the PPSDs for each component of motion are plotted together. The average difference in noise between each component of motion is about 3dB. We note that while the time domain analysis of the outliers in Figure 4 suggests that noise levels in the 10-20cm range are not uncommon, the frequency domain analysis shows a more nuanced perspective. At shorter periods, shorter than 100s, which are comparable with the duration of large earthquake, noise is much closer to the ~5cm level. Meanwhile at shorter periods than that (e.g. 10s) 1cm or even sub-cm level noise is prevalent.

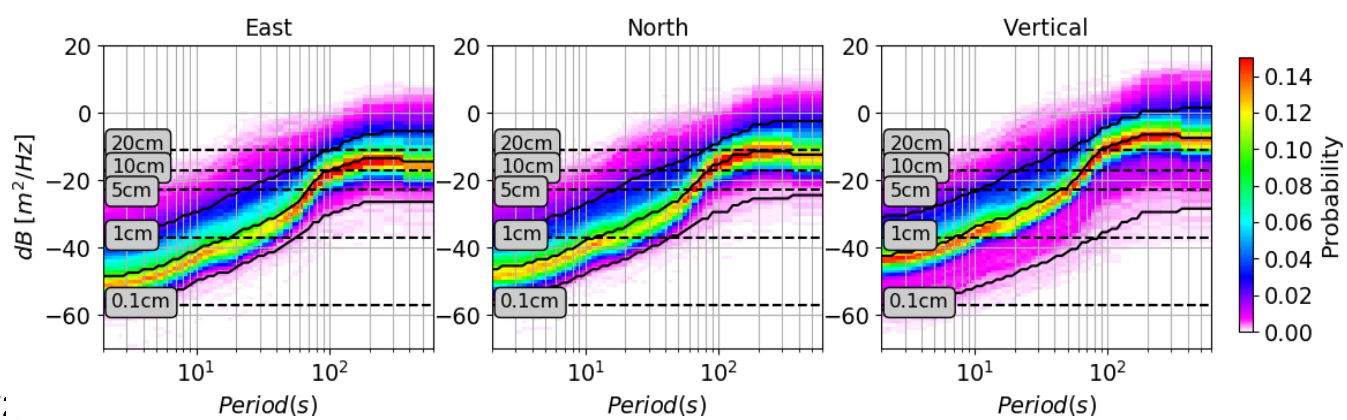

***Figure 5**. Aggregate PPSDs for the three components of motion for all stations in this study. The continuous black lines denote the 1th, 50th, and 90th percentiles. The dashed*

lines are used as a reference and denote the power of a time series of Gaussian white noise with specified standard deviation.

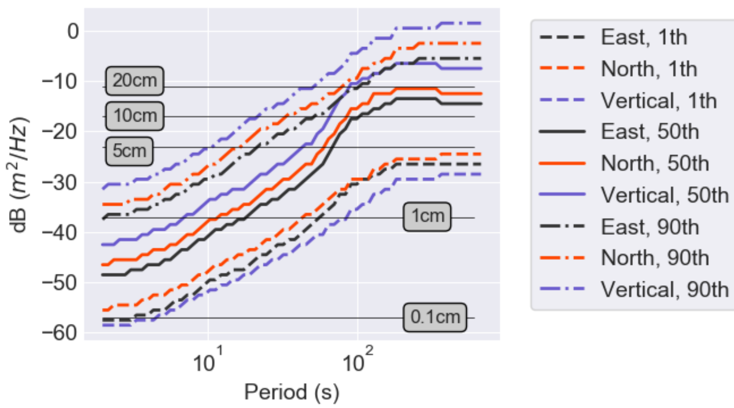

***Figure 6**. Comparison plot of the 1th, 50th, and 90th percentiles of the PPSD noise distribution for all sites from Figure 5. The horizontal thin black reference lines are used as a reference and denote the power of a time series of Gaussian white noise with specified standard deviation*

<u>3.2 Spatiotemporal characteristics of noise</u>

We are also interested in the variations of the noise distribution over long periods of time. Figure 7 shows the spectrogram for the nearly year-long time series at station BILS and for a period of 1 week. We find that, while there can be short periods of higher or lower noise overall, the general spectral shape and the behavior of the noise is somewhat stable. At a particular period the average standard deviation of the PSD throughout the year is only 5-6dB with larger excursion from this baseline behavior occurring only over short periods of time (e.g. P1 in Figures 7 and 8). The time series of power at selected periods, also shown in Figure 7, hint at regular variations in the noise behavior and also suggest that the temporal changes to the noise covary between periods. This is especially obvious in the week long time series. In Figure 9 we explore this further, we extract the time series of power spectral density at these 3 periods (2s, 60s, and 300s) for each site and calculate the spectra for each. We then stack them across all the sites to see if there are any spectral peaks that are systematically present at all sites. There are several (Figure 9), of particular prominence we note peaks at 1.96hrs, 11.38hrs and 21-23hr periods. This “spectra of spectra” should not be interpreted to suggest position signals at these periods, rather they show that with a periodicity of, for example ~2hrs, the entire spectra of the positions at all frequencies shift wholesale to higher or lower noise levels. The spectra explains some of the temporal variability in the noise behavior but we note, and will discuss further on, that the time series are punctuated by short periods of very high noise (e.g. P1 in Figures 7 and 8) that occur at irregular intervals.

We also explore the spatial distribution of noise across the sites. Figure 10 is a map of the amplitude of the noise at a period of 60s across the entire network. We do not observe any strong spatial pattern with respect to preferential locations or environments for low or high noise sites. For example in the Southern California cluster there are many low noise sites (~-26dB) however, in between many of them are interspersed high noise sites with power closer to -22dB or -21dB. The same is true in the other three clusters in the Bay area, the Pacific Northwest, and Alaska. Additionally we do not observe systematically higher noise in any of the regions shown in Figure 10.

<u>*3.3 Synthetic noise time series*</u>

Figure 6 exemplifies three potential reference noise models from which to choose. We define the 1th percentile model as the "low" noise model, the 50th percentile as the "median" model, and the 90th percentile as the high noise model. These can be used to generate arbitrarily long synthetic time series of noise to be injected into simulations of earthquakes or any other potential application where high-rate positions are used or required [e.g. Melgar et al., 2016]. Figure 11 shows by way of an example a three component 20 minute time series of median synthetic noise compared to a twenty minute window from station BILS. The figure illustrates that the two are, as designed, very similar to each other.

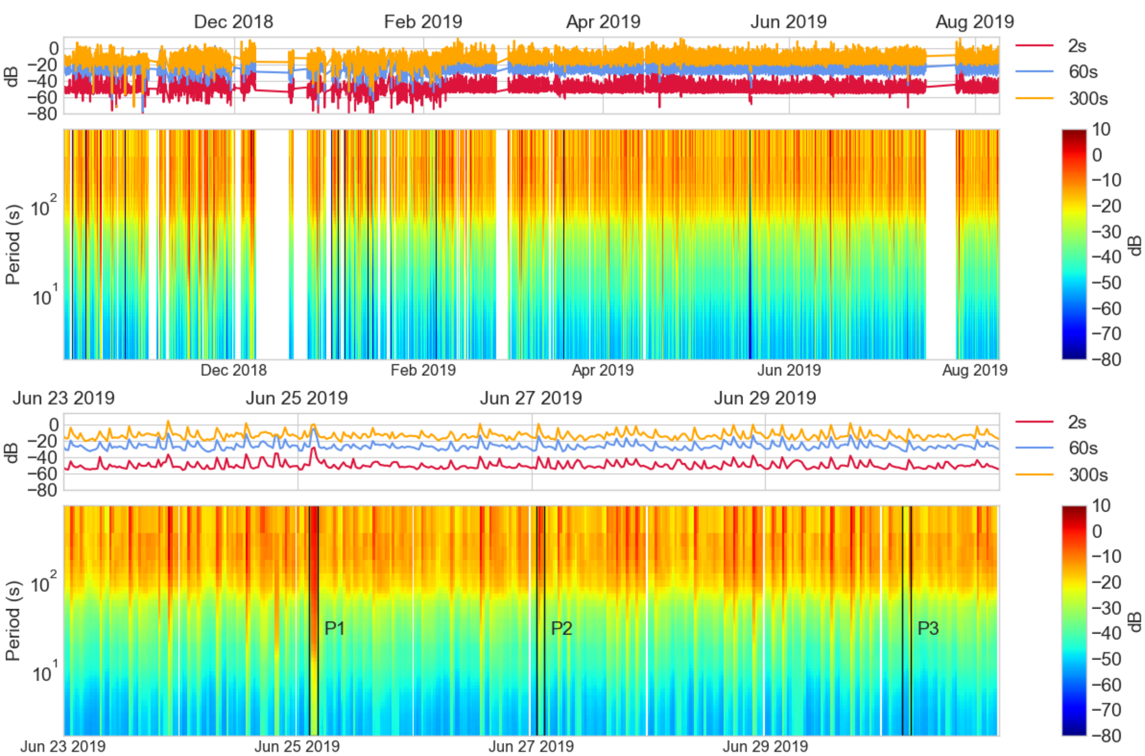

***Figure 7**. Top, year long spectrogram of positions for the east component of station BILS (Figure 2). For ease of interpretation we also plot the time series of power for 3 selected periods, 2s, 60s, and 300s. Bottom, same as the top but for a shorter time span of only 1 week. The time periods labeled P1, P2, P3 enclosed in the rectangles*

correspond to periods of high, medium, and low noise. Time series for these periods are in Figure 8.

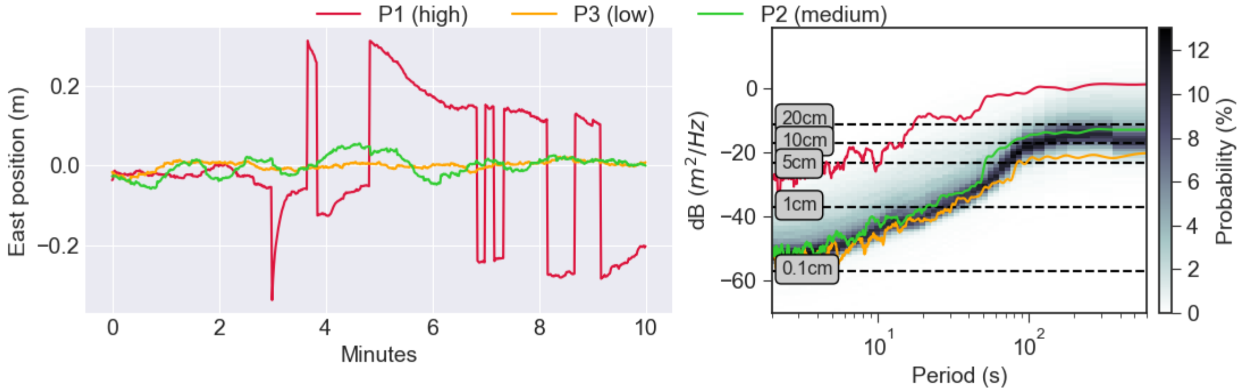

***Figure 8**. Left: Example 10 minute long time series for periods of high, medium, and low noise for the east component of station BILS. The time periods are highlighted as P1, P2, and P3 in the spectrogram on Figure 7. Right: PPSD for station BILS, (same as Figure 3) with spectra for noise at time periods P1, P2, and P3. The dashed lines are used as a reference and denote the power of a time series of Gaussian white noise with specified standard deviation*

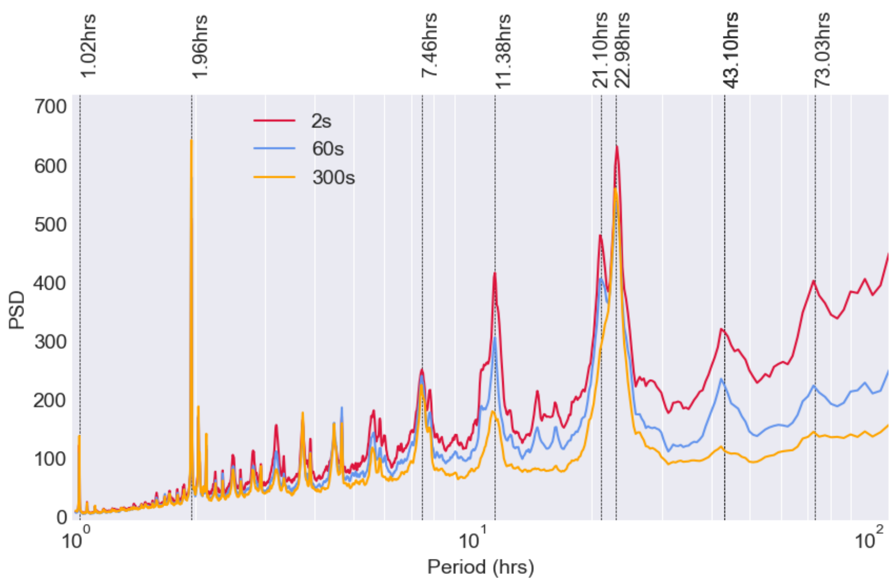

***Figure 9**. Stacked spectra of the time series of power of the noise at 2s, 60s, and 300s periods (see Figure 7). The individual spectra for each site are calculated for the entire time span and then all the sites are averaged together to create the stack.*

4. Discussion

4.1 On the characteristics of the noise

Langbein & Bock [2004] and Genrich & Bock [2006] first analyzed the noise behavior of HR-GNSS positions obtained from relative positioning (where the positions are with respect to a reference site). Those studies found that noise has a characteristic "dam" profile, with approximately flat power at long periods and linearly decaying (in a log-log sense) power at higher frequencies. In this study we find that positions obtained from PPP are consistent with these earlier findings. At periods longer than ~200s power is mostly flat, suggesting mostly uncorrelated positions, with power decaying with a slope of -2 at shorter periods (e.g. Figures 5 and 6). This power of 2 decay is characteristic of a random walk process (e.g. Agnew 1992). Both the slope and the location of the spectral "corner" are consistent with earlier findings from Genrich & Bock [2006] who analyzed instantaneous relative positions for three baselines in Southern California. It suggests that the primary source in the short period band up to ~200s is a combination of the troposphere and multipath. At very short periods (<5s) there is an indication that the spectra are beginning to flatten, this too would be consistent with Genrich & Bock [2006] and Bock et al. [2011] who observed mostly white noise in 50Hz sampled GNSS at periods shorter than 1-2Hz. This white noise behavior is indicative that the noise sources at these higher frequencies are uncorrelated.

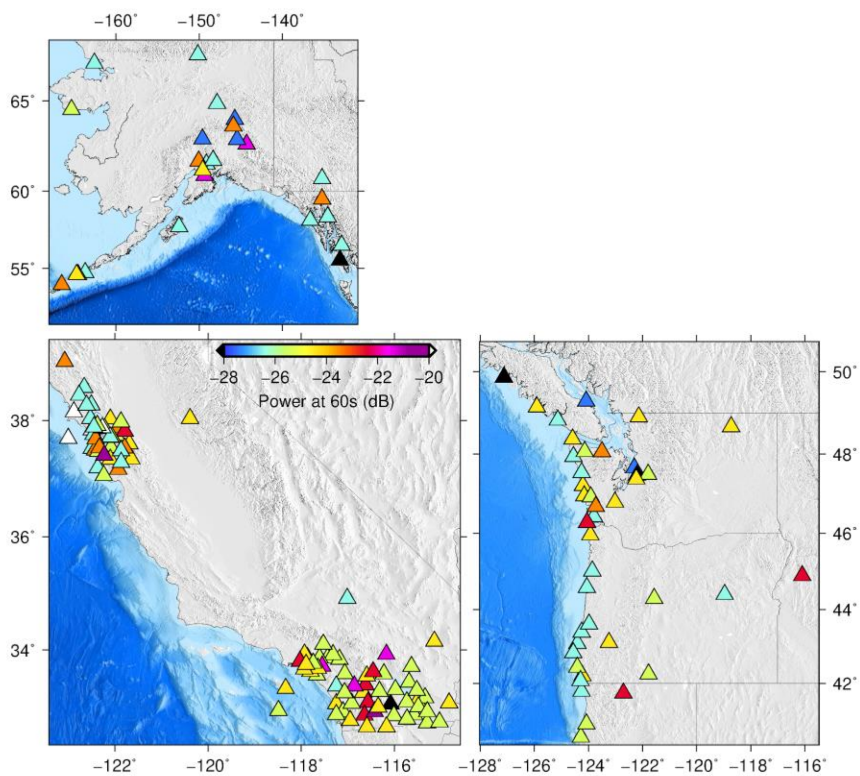

***Figure 10**. Distribution of noise at 60s period in the California, Pacific Northwest and Alaska regions.*

The long term behavior of the noise in Figure 7 is interesting. The spectrograms show a periodic variability in the noise levels which is punctuated by irregularly spaced short intervals of time where there is a wholesale increases or decrease of noise. The time series of power in Figure 7 were collected at 2s, 60s, and 300s, which alternatively correspond to the short period somewhat flattened part of the spectrum, the linearly decaying part of the spectrum, and the long period approximately flat part of the spectrum. The changes in power at all of these periods co-vary, even during periods (such as P1 in Figure 7) when there are large increases in noise. This is perhaps unsurprising, Figure 8 shows that the noise increase is manifested as several step-like jumps, likely from errors in the ambiguity resolution procedure. We also see a gradual decay after each step offset which is characteristic of "re-convergence" after a cycle slip (e.g. Geng et al., 2013).

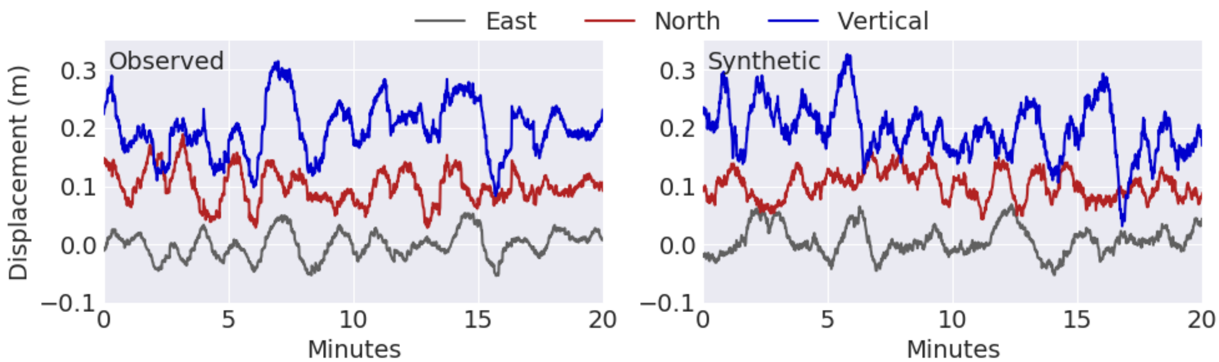

Figure 11, *20 minutes of noise observed at station BILS (Figure 2) and 20 minutes of synthetic noise generated using the median noise model from Figure 5. The time series for each direction of motion are offset for clarity.*

The irregular distribution of station noise in Figure 10 is somewhat surprising and will warrant further study. A priori one would expect a geographic correlation between the noise levels and a number of potential candidate parameters. For example it is well known that the geometry of the constellation of GPS satellites is less favorable for positioning at higher latitudes. Similarly the ionosphere should be more active as one approaches the poles. Yet we do not observe a systematic degradation of the northern sites. Similarly, one would expect that multipath would correlate strongly with the noise performance of the stations. We also do not see a correlation between noise power and the signal to noise ratio in the L1 and L2 frequencies. We explore this further in Figure 12. Here we plot the time series of power at 60s period for a 4 day period for all sites in the San Francisco Bay Area cluster. We see clearly that in this limited geographic region over length scales of ~100km the noise at many sites is highly correlated. Both episodes of elevated and reduced noise occur close together in time between many sites. We calculate the correlation coefficient of all the time series to an arbitrary site in the middle of the cluster (P223) and indeed we find high correlation (>0.75) between many of the stations. This is true even for station CMBB which is 175km from P223 and still exhibits a high (0.7) correlation coefficient. In Figure 12 we also show the median power at 60s period for the same 4 day period. We see clearly that the stations that do not follow the same regional variation in noise are those with highest power. These noisy sites have a completely different evolution of noise with time.

Figures 10 and 12 show that a likely explanation for the noise behavior at a particular site is a weighted sum of many factors The strong correlations at ~100km length scales are evidence of regional effects. This includes period of disturbances in both the ionospheric and troposphere which would affect stations over regions of this size. Similarly drifts in clocks and orbits will have a strong regional correlation. However, that the absolute level of the noise at stations analyzed in this study exhibits poor correlation with obvious geographic features strongly suggests that this is an effect local to each site. The quality of the monument, and the environment (vegetation, snow, buildings, other microwave equipment) surrounding each site is highly heterogeneous and can have an outsized effect in the positioning quality raising the noise floor substantially.

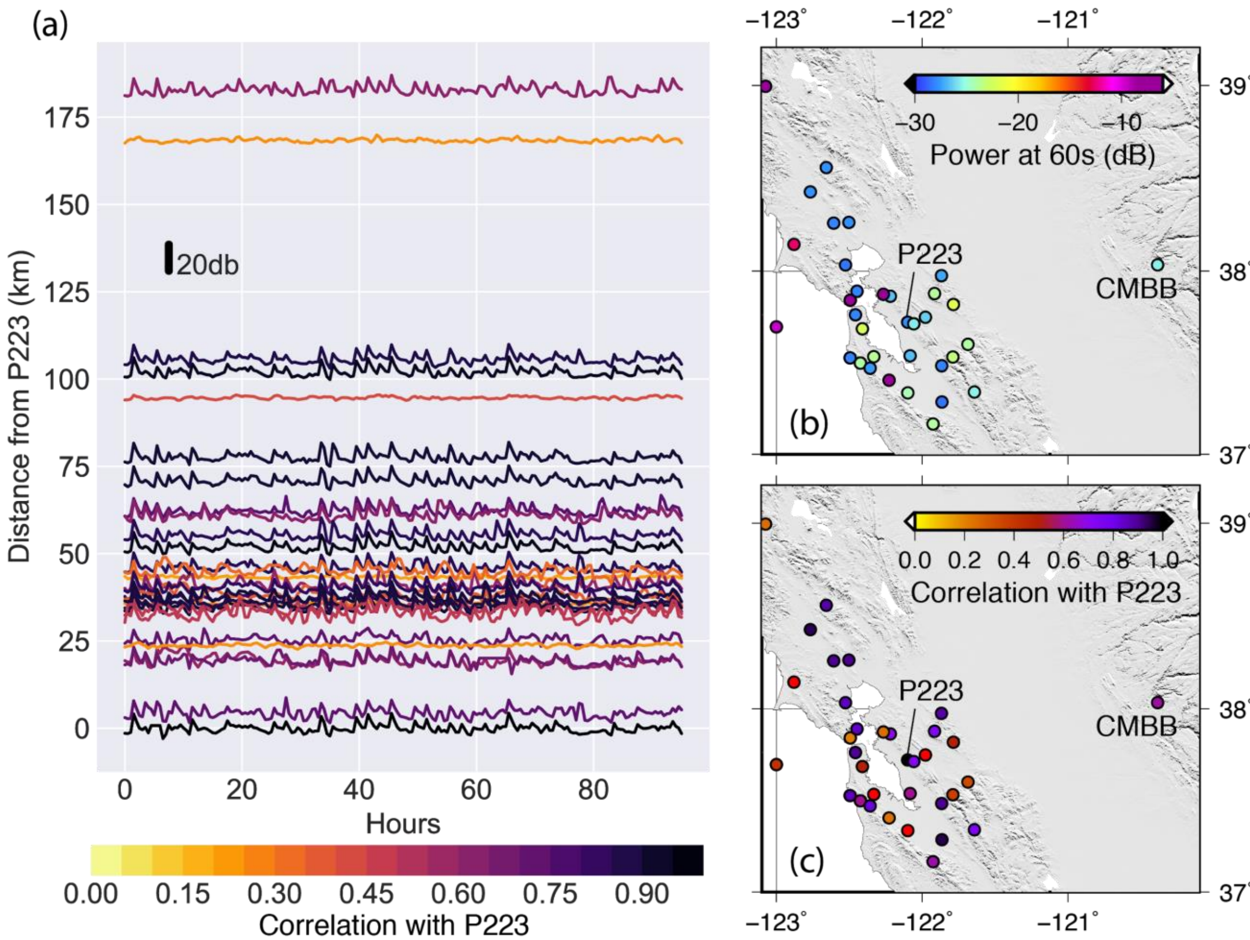

Figure 12. *(a) Time series of power at 60s period for the 4 day time span from June 26th to June 30th 2019 for station in the San Francisco Bay Area cluster. The time series are colored by the correlation coefficient to a reference site inside the cluster (station P223) (b) Locations of the stations in the cluster and median power at 60s period for the selected time span. (c) Correlation between all sites to reference station P223.*

Finally we note that there are other noise sources which will be specific to the positioning algorithm being used. For example the ~2hr peak (Figure 9) is likely due to the frequency with which the orbital parameters in the broadcast ephemeris are updated by IGS. These updated values are used in the FastLane processing scheme and introduce a regular periodic behavior. Indeed an important point we stress is that the overall noise behavior and shape of the spectra should roughly follow the “dam” profile irrespective of the positioning algorithm being used. However the details of the noise behavior will be strongly influenced by not just the traditional sources of noise but also by the processing strategy. Deviations from the noise behavior we detail here should not be unexpected.

4.2 Implications for positioning algorithms

The noise models we propose are useful signposts which can be used to compare against as improvements to GNSS positioning technologies are developed. For example broadcast of new frequencies by GNSS satellites [Geng & Bock, 2013; Zhao et al., 2015], and positioning strategies that harness multiple constellations (“true GNSS”) promise to provide substantial improvements and reductions in noise [Odolinski et al., 2015; Geng et al., 2016; Geng et al., 2019b]. As this technology is incorporated into permanent monitoring networks it can be evaluated by comparison to established baselines of noise behavior.

4.3 Comparison to seismological noise

The concepts behind this study were inspired by the techniques proposed by McNamara & Buland [2004] who carried out a similar analysis for noise at seismic sites in the continental United States and established its systematic behavior. Because use of HR-GNSS is becoming widespread in monitoring efforts in seismology we have attempted to establish a similar baseline of behavior here. However, some critical conceptual differences warrant a few comments. The background seismic noise observed at broadband sites on-land are actual vibrations of the ground whose source is the interactions of the oceans with the near-shore solid Earth (e.g. Longuet Higgins, 1950). This noise is of comparatively very small amplitude, at periods of 1s, for example, it is expected to have a power of -170 to -130 dB [Peterson, 1993]. This is several orders of magnitude below what we measure from GNSS (-55dB, Figure 5). We emphasize that the source of noise in GNSS positions have nothing to do with actual high-frequency motions of the ground. It is true that longer period deformation of the Earth such as that induced by tides can have mm to sub-mm amplitudes (e.g. Agnew, 2010) however this is outside the frequency band of interest to monitoring large earthquakes. Rather, most of the noise comes from the variable delays to the microwave satellite signals introduced by the troposphere and ionosphere and spurious reflections (multipath) of the microwaves off of the surrounding terrain which occlude the main arrival to the GNSS antenna. Another large source of noise is imperfect knowledge in real-time of the satellite clocks and orbits. Long period noise induced by constellation geometry is highly repeatable and can be reduced through sidereal filtering [Larson et al., 2007]. Assuming that technical improvements in mitigating these noise sources are possible this large gap (~70dB) between background seismic noise and current GNSS noise suggests that the lower bound of what could be observed lies far beyond what is possible now. There is essentially unbounded room for improvement.

4.4 Implications for seismic monitoring

Previous studies of the relative amplitudes of ground displacements at regional distances from medium to large events [Crowell et al., 2013, Melgar et al., 2015, Ruhl et al., 2018] suggest that, in order for GNSS time series to be of use for monitoring, precision of a few centimeters is necessary. For example, if the precision were relatively poor, say 10cm, the peak ground displacement scaling laws of Melgar et al. [2015] predict that an M7 earthquake would be visible to any site within 91km. That distance grows to 462km and 1628km for M8 and M9 earthquakes respectively. The aggregate PPSDs in Figures 5 and 6 then suggest that the current precision achieved by the real-time GNSS solutions is sufficient for monitoring large events.

Figure 13 shows an example of the potential performance. There we plot the three component HR-GNSS displacements for station CCCC which was processed in real-time with Fastlane and recorded both the M6.4 and M7.1 Ridgecrest CA earthquakes at 35 and 50km from the source [Melgar et al., 2019; Goldberg et al, 2019]. We also plot the spectra for the waveforms and the median noise models. This shows clearly that the waveforms are reliable. Melgar et al. [2019] showed that while there were some small but appreciable differences between the real-time and post-processed high-rate solutions the features of the waveforms most used in monitoring remained consistent in both sets of solutions.

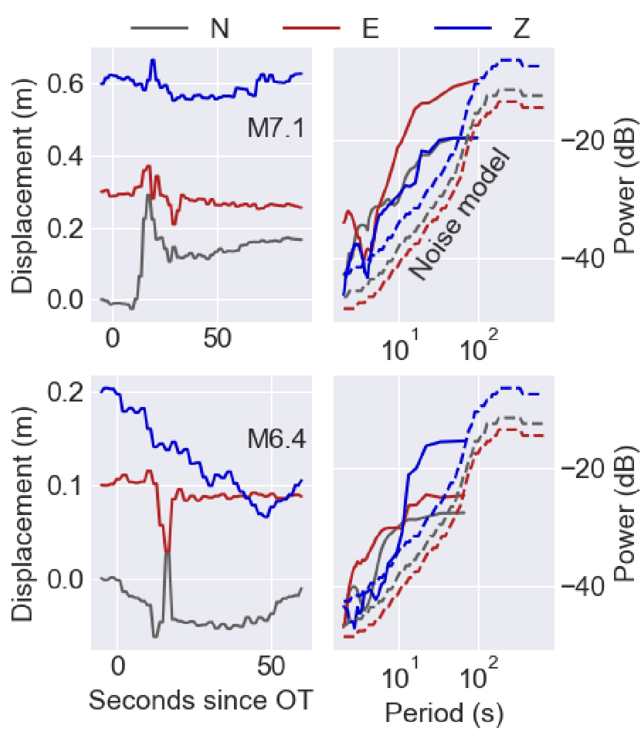

Figure 13. *Real-time three-component displacements at station CCCC during the 2019 M6.4 and M7.1 Ridgecrest CA earthquakes plotted as seconds since the*

earthquake origin time (OT). Also shown are the spectra of the waveforms compared to the median noise model

Another important use of the work discussed here for monitoring is in making objective and automated assessments of the station positioning quality. Figure 8 exemplifies how an otherwise well-behaved station can, for limited periods of time, have elevated noise levels which can have detrimental effects on any algorithm using it to model an earthquake source. Monitoring agencies can use either the global noise model, or a station by station noise model, and set percentile cutoffs, perhaps at a few selected periods. If the noise rises above that threshold for some period of time the station can be quarantined or "black listed" so that it doesn't contribute solutions to a source modeling algorithm should an earthquake occur in that time. Later as the station noise drops to an acceptable level it can be removed from the black list. Similarly sites that are routinely above some threshold level will likely need to be serviced or altogether removed from contribution to any real-time monitoring effort.

For the Fastlane algorithm in particular one important challenge remains as it continues to contribute solutions to monitoring agencies. The large outliers seen in Figure 2 are not the norm (e.g. Figure 4) but they are large enough that should they occur during an earthquake they could introduce significant errors into the modeling. This is problem has been noted in real-time monitoring efforts elsewhere [Kawamoto et al., 2017]. This in general will not be an issue for the computation of coseismic offsets, as a moving average or median filters can be employed (i.e., Crowell et al. [2016]), however, for PGD scaling, significant outliers or cycle slips can influence the derived magnitude estimates. During the Ridgecrest earthquakes there were no occurrences of this in any of the real-time waveforms. However continued effort in making the positioning strategy more robust is ongoing.

5. Conclusions

Large earthquakes are difficult to model in real-time with traditional inertial seismic measurements. Several algorithms that leverage high-rate RT-GNSS positions have been proposed and it has been shown that they can supplement the earthquake monitoring effort. However, analyses of the long-term noise behavior of high-rate RT-GNSS positions, which are important to understand how the data can be used operationally by monitoring agencies, have been limited to just a few sites and to short time spans. Here we have shown results from an analysis of the noise characteristics of one year of positions at 213 RT-GNSS sites spanning a large geographic region from Southern California to Alaska. We have characterized the noise and proposed several references noise models which can be used as baselines to compare against as technological improvements allow for higher precision solutions. We have also shown how to use the reference noise models to generate realistic synthetic noise that can be used in simulations of HR-GNSS waveforms. Additionally, we find that while variations in the noise have a strong spatial correlation the absolute level of noise at a site does not. This is evidence that local effects (monumentation, station conditions, multipath etc.) likely dominate the noise behavior.

Further, we have shown how this noise analysis can be used in a dynamic quality control to determine which sites should or should not contribute positions to an earthquake modeling algorithm at a particular moment in time. Overall, while there remain important improvements yet to be made, such as reducing the number of outliers, we find that the present quality of real-time HR-GNSS waveforms is more than sufficient for monitoring large earthquakes.

Acknowledgments

Development of global GNSS seismic analyses is supported by NASA-ESI awards NNX14AQ40G & 80NSSC19K0359 and USGS Cooperative Agreements G17AC00344 & G19AC00264 to Central Washington University. Analysis of the real-time data is supported by NASA grants 80NSSC19K0360 and 80NSSC19K1104, and NSF grant OAC1835661 to the University of Oregon. Some data are from Network of the Americas (NOTA) stations, funded by the National Science Foundation and operated by UNAVCO, Inc. Data based on services provided by the GAGE Facility, operated by UNAVCO, Inc. with support from the National Science Foundation and the National Aeronautics and Space Administration under NSF Cooperative Agreement EAR-1724794. Additional data for this study come from the Bay Area Regional Deformation Network (BARD), doi:10.7932/BARD, operated by the UC Berkeley Seismological Laboratory, which is archived at the Northern California Earthquake Data Center (NCEDC), doi: 10.7932/NCEDC. The synthetic GNSS noise generation code can be found at, https://github.com/dmelgarm/MudPy and a tutorial on how to run the code is at https://github.com/dmelgarm/MudPy/wiki/Generate-synthetic-HR-GNSS-noise

References

Agnew, D.C., (1992). The time‐ domain behavior of power‐ law noises. Geophysical research letters, 19(4), pp.333-336.
Agnew, D.C., (2010). Earth Tides. Treatise on Geophysics, Volume 3: Geodesy, p.163.
Altamimi, Z., P. Rebischung, L. Metivier, and X. Collilieux (2016), ITRF2014: A new release of the International Terrestrial Reference Frame modeling nonlinear station motions, J. Geophys. Res. Solid Earth, 121, doi:10.1002/2016JB013098.
Barrientos, S. and Pérez‐ Campos, X., (2018). Preface to the Focus Section on Geophysical Networks and Related Developments in Latin America. *Seism. Res. Lett.*, 89(2A), pp.315-317.
Blewitt, G., W. C. Hammond, and C. Kreemer (2018), Harnessing the GPS data explosion for interdisciplinary science, Eos, 99, https://doi.org/10.1029/2018EO104623.
Bock, Y., Nikolaidis, R.M., de Jonge, P.J. and Bevis, M., (2000). Instantaneous geodetic positioning at medium distances with the Global Positioning System. Journal of Geophysical Research: Solid Earth, 105(B12), pp.28223-28253.
Bock, Y., Melgar, D. and Crowell, B.W., (2011). Real-time strong-motion broadband displacements from collocated GPS and accelerometers. Bulletin of the Seismological Society of America, 101(6), pp.2904-2925.

Bock, Y. and Melgar, D., (2016). Physical applications of GPS geodesy: A review. Reports on Progress in Physics, 79(10), p.106801.

Boore, D.M., (1983). Stochastic simulation of high-frequency ground motions based on seismological models of the radiated spectra. Bulletin of the Seismological Society of America, 73(6A), pp.1865-1894.

Crowell, B.W., Melgar, D., Bock, Y., Haase, J.S. and Geng, J., 2013. Earthquake magnitude scaling using seismogeodetic data. Geophysical Research Letters, 40(23), pp.6089-6094.

Crowell, B.W., Schmidt, D.A., Bodin, P., Vidale, J.E., Gomberg, J., Renate Hartog, J., Kress, V.C., Melbourne, T.I., Santillan, M., Minson, S.E. and Jamison, D.G., (2016). Demonstration of the Cascadia G- FAST geodetic earthquake early warning system for the Nisqually, Washington, earthquake. Seismological Research Letters, 87(4), pp.930-943.

Fang, R., Shi, C., Song, W., Wang, G. and Liu, J., (2013). Determination of earthquake magnitude using GPS displacement waveforms from real-time precise point positioning. Geophysical Journal International, 196(1), pp.461-472.

Geng, J., Bock, Y., Melgar, D., Crowell, B.W. and Haase, J.S., (2013). A new seismogeodetic approach applied to GPS and accelerometer observations of the 2012 Brawley seismic swarm: Implications for earthquake early warning. Geochemistry, Geophysics, Geosystems, 14(7), pp.2124-2142.

Geng, J. and Bock, Y., (2013). Triple-frequency GPS precise point positioning with rapid ambiguity resolution. Journal of Geodesy, 87(5), pp.449-460.

Geng, T., Xie, X., Fang, R., Su, X., Zhao, Q., Liu, G., Li, H., Shi, C. and Liu, J., (2016). Real- time capture of seismic waves using high- rate multi- GNSS observations: Application to the 2015 Mw 7.8 Nepal earthquake. Geophysical Research Letters, 43(1), pp.161-167.

Geng, J., Chen, X., Pan, Y., Mao, S., Li, C., Zhou, J. and Zhang, K., (2019a). PRIDE PPP-AR: an open-source software for GPS PPP ambiguity resolution. GPS Solutions, 23(4), p.91.

Geng, J., Guo, J., Chang, H. and Li, X., (2019b). Toward global instantaneous decimeter-level positioning using tightly coupled multi-constellation and multi-frequency GNSS. Journal of Geodesy, 93(7), pp.977-991.

Genrich, J.F. and Bock, Y., (2006). Instantaneous geodetic positioning with 10–50 Hz GPS measurements: Noise characteristics and implications for monitoring networks. Journal of Geophysical Research: Solid Earth, 111(B3).

Goldberg, D. E., Melgar, D., Thomas, A., Sahakian, V. J., Xu, X., Geng, J., & Crowell, B. W. (2019). Complex Rupture of an Immature Fault Zone: A Simultaneous Kinematic Model of the 2019 Ridgecrest, CA Earthquakes. EarthArXiv, doi:10.31223/osf.io/s79bk

Grapenthin, R., Johanson, I.A. and Allen, R.M., (2014). Operational real- time GPS-enhanced earthquake early warning. Journal of Geophysical Research: Solid Earth, 119(10), pp.7944-7965.

Graves, R.W. and Pitarka, A., (2010). Broadband ground-motion simulation using a hybrid approach. Bulletin of the Seismological Society of America, 100(5A), pp.2095-2123.

Hoshiba, M. and Ozaki, T., (2014). Earthquake Early Warning and Tsunami Warning of the Japan Meteorological Agency, and Their Performance in the 2011 off the Pacific Coast of Tohoku Earthquake (Mw9.0). In Early warning for geological disasters (pp. 1-28). Springer, Berlin, Heidelberg.

Kawamoto, S., Ohta, Y., Hiyama, Y., Todoriki, M., Nishimura, T., Furuya, T., Sato, Y., Yahagi, T. and Miyagawa, K., (2017). REGARD: A new GNSS- based real- time finite fault modeling system for GEONET. Journal of Geophysical Research: Solid Earth, 122(2), pp.1324-1349.

Kouba, J. and Héroux, P., (2001). Precise point positioning using IGS orbit and clock products. GPS solutions, 5(2), pp.12-28.

Langbein, J. and Bock, Y., (2004). High- rate real- time GPS network at Parkfield: Utility for detecting fault slip and seismic displacements. Geophysical Research Letters, 31(15).

Larson, K.M., Bilich, A. and Axelrad, P., (2007). Improving the precision of high- rate GPS. Journal of Geophysical Research: Solid Earth, 112(B5).

Larson, K.M., (2019). Unanticipated Uses of the Global Positioning System. Annual Review of Earth and Planetary Sciences, 47(1) , pp. 19-40.

Longuet-Higgins, M.S., (1950). A theory of the origin of microseisms. Philosophical Transactions of the Royal Society of London. Series A, Mathematical and Physical Sciences, 243(857), pp.1-35.

McNamara, D.E. and Buland, R.P., (2004). Ambient noise levels in the continental United States. Bulletin of the seismological society of America, 94(4), pp.1517-1527.

Melbourne, T.I, Stough, T., Bar-Sever, Y., Bock, Y., Song, T. (2018), Operationalizing GNSS as a Fourth Observation for Local Tsunami Warning, Abstract NH34B-02 presented at 2018 Fall Meeting, AGU, Washington, D.C., 10-14 Dec.

Melgar, D., Crowell, B.W., Geng, J., Allen, R.M., Bock, Y., Riquelme, S., Hill, E.M., Protti, M. and Ganas, A., (2015). Earthquake magnitude calculation without saturation from the scaling of peak ground displacement. Geophysical Research Letters, 42(13), pp.5197-5205.

Melgar, D., Melbourne, T.I., Crowell, B.W., Geng, J., Szeliga, W., Scrivner, C., Santillan, M., Goldberg, D.E., (2019). Real-time High-rate GNSS Displacements: Performance Demonstration During the 2019 Ridgecrest, CA Earthquakes. EarthArXiv, doi:10.31223/osf.io/pdxqw.

Minson, S.E., Murray, J.R., Langbein, J.O. and Gomberg, J.S., (2014). Real- time inversions for finite fault slip models and rupture geometry based on high- rate GPS data. Journal of Geophysical Research: Solid Earth, 119(4), pp.3201-3231.

Odolinski, R., Teunissen, P.J. and Odijk, D., (2015). Combined bds, galileo, qzss and gps single-frequency rtk. GPS solutions, 19(1), pp.151-163.

Peterson (1993). Observation and modeling of seismic background noise, U.S. Geol. Surv. Tech. Rept. 93-322, 1–95.

Riquelme, S., Bravo, F., Melgar, D., Benavente, R., Geng, J., Barrientos, S. and Campos, J., (2016). W phase source inversion using high- rate regional GPS data for large earthquakes. Geophysical Research Letters, 43(7), pp.3178-3185.

Ruhl, C.J., Melgar, D., Geng, J., Goldberg, D.E., Crowell, B.W., Allen, R.M., Bock, Y., Barrientos, S., Riquelme, S., Baez, J.C. and Cabral- Cano, E., (2018). A global database of strong- motion displacement GNSS recordings and an example application to PGD scaling. Seismological Research Letters, 90(1), pp.271-279.

Santillan, M., Melbourne, T., Szeliga, W., Scrivner, V., (2013) A fast-convergence stream editor for real-time Precise Point Positioning, annual meeting of the American Geophysical Union, San Francisco, CA, Abstract G53B-0930

Zhao, Q., Sun, B., Dai, Z., Hu, Z., Shi, C. and Liu, J., 2015. Real-time detection and repair of cycle slips in triple-frequency GNSS measurements. GPS Solutions, 19(3), pp.381-391.

Zumberge, J.F., Heflin, M.B., Jefferson, D.C., Watkins, M.M. and Webb, F.H., (1997). Precise point positioning for the efficient and robust analysis of GPS data from large networks. Journal of geophysical research: solid earth, 102(B3), pp.5005-5017.